

Pinhole imaging to observe spatial jitters of a triple-pulse X-ray source on the Dragon-II LIA

Yi Wang¹ · Zhi-Yong Yang¹ · Xiao-Bing Jing¹ ·
Qin Li¹ · Heng-Song Ding¹ · Zhi-Yong Dai¹

Received: 25 January 2016/Revised: 7 April 2016/Accepted: 14 April 2016/Published online: 26 August 2016
© Shanghai Institute of Applied Physics, Chinese Academy of Sciences, Chinese Nuclear Society, Science Press China and Springer Science+Business Media Singapore 2016

Abstract In high-energy flash radiography, scattered photons degrade the acquiring image, which limits the resolving power of interfaces and density of dense object. The application of large anti-scatter grid can reduce the scattered photons remarkably, but this requires a stable source position in order to reduce the loss of signal photons in the grid structure. The pinhole imaging technique is applied to observe spatial jitters of a triple-pulse radiographic source of a linear induction accelerator. Numerical simulations are conducted to analyze the imaging performance with the same or close parameters of the pinhole object and experimental alignment. Experiments are carried out to observe spatial jitters of the source between different measurements. Deviations of the source position between different pulses are measured in each experiment.

Keywords Spatial jitter · X-ray source · Pinhole imaging · Linear induction accelerator

1 Introduction

Flash radiography is an extraordinary diagnostic technique to investigate the hydrodynamic process of high explosives [1]. The radiographic source is generally produced by a linear induction accelerator (LIA). Electron

beam pulses are accelerated to \sim MeV and focused onto a high-Z convertor target to generate X-rays (bremsstrahlung) [2–6]. The temporal width of an E-beam pulse is usually tens of nanoseconds, which enables a recording of an inner stopped-motion image of a dense object. In flash radiography, photon scattering is a major obstacle for acquiring fine details of interfaces and object density [7, 8].

Efforts were devoted to investigations of photon scatter properties and anti-scatter techniques, including various kinds of collimators made of heavy materials to reduce scatter background and improve contrast in radiography [9–11]. However, the collimators placed between the object and the light source is usually accompanied with a loss of abaxial image information of the object. The Los Alamos National Laboratory developed a structure of large anti-scatter grid of high grid ratios, and the scattered photons can be remarkably reduced for radiography [12]. The scintillator array of image-receiving system is directly pinned to the grid, the correspondence of which is perfectly matched to be one-scintillator-pixel to one-grid-hole. Since the anti-scatter grid is designed to fit the directions in which radiation photons are emitted, it ought to be strictly aligned to focus exactly at the center of the light source. A spatial jitter of the source can result in a loss of primary radiation in the grid structure [13]. The higher the grid ratio is, the more sensitively the source spatial jitter would degrade the image.

In this paper, the pinhole imaging technique [14, 15] is applied to measure spatial position of a triple-pulse X-ray source produced by the Dragon-II LIA. The acquiring image denotes a two-dimensional distribution of the X-ray source, by which the spatial position of the source centroid can be obtained. Experiments are performed to observe spatial jitters of the source between different measurements. The

✉ Yi Wang
wangyi_caep@163.com

¹ Key Laboratory of Pulsed Power, Institute of Fluid Physics, China Academy of Engineering Physics, Mianyang 621900, China

interpulse differences of the source centroid are measured in each experiment.

2 Principle and setup

In flash radiography, photons from the X-ray source pass through the objects in the light field and finally reach the image-receiving system. The spatial distribution of radiographic image $i(x, y)$ is a convolution of the source spatial distribution $s(x, y)$, the transmitted intensity distribution of object $o(x, y)$, and the detector response to a point X-ray source $r(x, y)$, i.e.,

$$i(x, y) = s(x, y) * o(x, y) * r(x, y), \quad (1)$$

where the sign $*$ denotes the convolution operation. The modulation transfer function (MTF) of a radiographic system is simply the product of MTFs of each component [16], and a Fourier transform of Eq. (1) can be done to obtain Eq. (2)

$$I(f_x, f_y) = S(f_x, f_y) \cdot O(f_x, f_y) \cdot R(f_x, f_y), \quad (2)$$

where I , S , O , and R stand for MTFs of each component in Eq. (1). A sketch of pinhole imaging setup is illustrated in Fig. 1. A pinhole object is placed between the X-ray source and the image-receiving system. For an ideal pinhole, the spatial intensity distribution $o(x, y)$ can be described by the delta function $\delta(x, y)$, which denotes the MTF of $O(f_x, f_y) = 1$. The geometrical magnification of the experimental arrangement M is defined as the ratio of the pinhole-image distance b to the source–pinhole distance a . If the blurring of image-recording system is ignored in the setup with a large magnification, the relation of the source MTF and the image MTF will be simplified as

$$I(f_x, f_y) \approx S(f_x, f_y). \quad (3)$$

So, spatial distribution of the image is exactly a reflection of the source. Then the relation between the source centroid $P_0(x, y)$ and the image centroid $P(x, y)$ can be expressed as

$$P_0(x, y) = -P(x, y)/M, \quad (4)$$

where the negative sign indicates opposite directions of the image position and the source position.

3 Numerical simulations

The precondition of a tenable relation between the source and image positions given by Eq. (4) is to image the source with an ideal pinhole, i.e., an infinitesimally small hole through an infinitesimally thin and completely opaque sheet [17]. This, however, cannot be realized in practice, especially with penetrating X-rays, so high-Z materials are used to construct the pinhole object, which ought to be thick enough to make the “opaque” sheet. The pinhole aperture cannot be too small either because the view field shall cover enough area of the source. Besides, the screen blur effect should be considered.

Here we perform numerical simulations to analyze the pinhole imaging process with the same or close parameters of the object and the experimental alignment. Monte Carlo method [18, 19] is applied to simulate the X-ray generation by striking an electron beam of 19.0 MeV onto a tantalum target of 1.2 mm thickness and transmitting the photons through a tungsten pinhole object of 65 mm thickness with an aperture of 0.47 mm. Then we calculate the convolution of the transmitted photon intensity distribution with the point-spread function (PSF) of the screen blur as the obtained image. The source–pinhole distance is $a = 1119$ mm and the pinhole-image distance is $b = 4681$ mm. The PSF of screen blur is assumed to a Gaussian function with the standard deviation of 0.7 mm, according to measurement result by the edge response technique [20].

In the simulation, a Gaussian function is used to model spatial distribution of the source, with the FWHM being 1.0 mm at first. The source center (x, y) is located (in mm) at $(2, 0)$, $(-2, 0)$, $(0, 2)$ or $(0, -2)$. For each simulation, the sampling amount is 10^6 . The simulated images are shown in Fig. 2. Because the pinhole imaging process is not rotationally symmetric when the source is laterally decentered, we calculate the image centroid within boundaries containing 90 or 50 % of the photon intensity sum (PIS). The corresponding source centroid is worked out according to Eq. (4). Table 1 shows the calculated source centroid (P_{0cal}) and the set source position (P_{0setl}). $\Delta L = |P_{0cal} - P_{0setl}|$, the distance between the calculated and the set source positions, is superior to 0.1 mm with a 2-mm source displacement from the origin. The source FWHMs of 1.5 and 2.0 mm are then calculated and listed in Table 1. The results of P_{0cal} show a good agreement with the results of P_{0setl} .

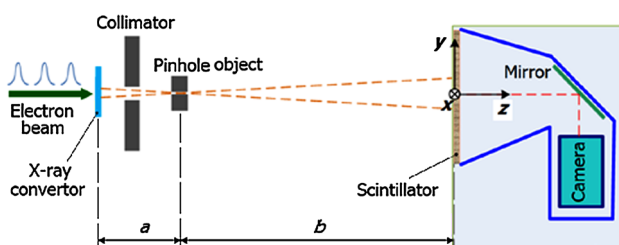


Fig. 1 Sketch of pinhole imaging setup

Fig. 2 Simulated pinhole images at different source positions (in mm). The white and the black dashes denote the boundaries of 90 % PIS and 50 % PIS, respectively. The source FWHM is 1.0 mm

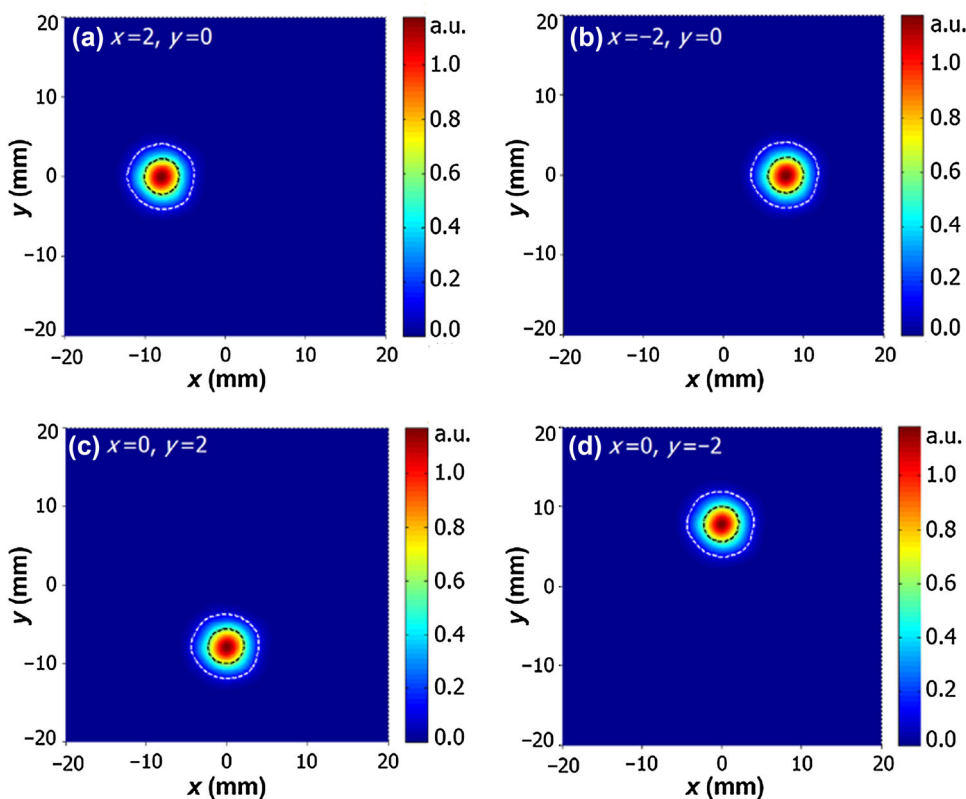


Table 1 Set and calculated source positions by numerical simulations (in mm)

Source FWHM	Set $P_0(x, y)$	Calculated $P_0(x, y)$			
		90 %PIS	ΔL	50 %PIS	ΔL
1.0	(2.000, 0.000)	(2.063, 0.002)	0.063	(2.056, 0.002)	0.056
	(-2.000, 0.000)	(-2.017, 0.001)	0.017	(-2.024, 0.003)	0.024
	(0.000, 2.000)	(0.022, 2.042)	0.047	(0.020, 2.046)	0.050
	(0.000, -2.000)	(0.022, -2.039)	0.044	(0.014, -2.044)	0.046
1.5	(2.000, 0.000)	(2.045, 0.005)	0.045	(2.034, -0.002)	0.034
	(-2.000, 0.000)	(-1.977, 0.000)	0.023	(-1.989, 0.005)	0.012
	(0.000, 2.000)	(0.034, 2.015)	0.037	(0.020, 2.010)	0.022
	(0.000, -2.000)	(0.031, -2.011)	0.033	(0.018, -2.009)	0.020
2.0	(2.000, 0.000)	(2.017, 0.004)	0.017	(1.995, -0.011)	0.012
	(-2.000, 0.000)	(-1.928, -0.002)	0.072	(-1.940, 0.004)	0.060
	(0.000, 2.000)	(0.044, 1.978)	0.049	(0.019, 1.967)	0.038
	(0.000, -2.000)	(0.040, -1.974)	0.048	(0.028, -1.972)	0.040

4 Measurements of the source position

Experiments are performed to observe the source position of the Dragon-II LIA, which generates triple X-ray pulses of ~ 60 ns in pulse length and ~ 400 -ns spacing between neighboring pulses. A lead collimator is placed just in front of the radiographic source as a radiation shield of the area away from the central field. A 65-mm-thick tungsten bar with a pinhole of 0.47 mm diameter is precisely placed along the central axis (z -axis). The image-

receiving system consists of an LYSO scintillator screen, a flat mirror tilted at 45° with respect to z -direction, and a framing camera to record each pulse image. The camera is composed of an optical framing element and several intensifier CCD cameras, and its gating time is controlled by a high-speed microchannel plank. Precisions of the trigger time and exposure time are less than 5 ns. By inputting external trigger synchronization signals, the camera records each pulse image separately. The experimental alignment is $a = 1119$ mm and $b = 4681$ mm,

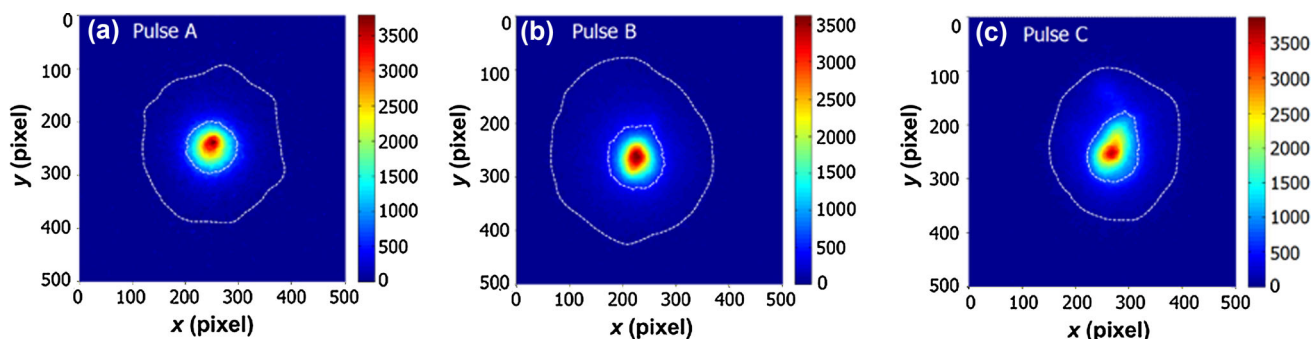


Fig. 3 Typical images of triple-pulse x-ray source by the pinhole method. The *inside* and *outside* curves denote the boundaries of 50 %PIS and 90 %PIS, respectively

Table 2 Experiment results of spatial position of the source centroid

Exp. no.	Pulses	E (MeV)	I (kA)	$P_0(x, y)$ (mm)	
				90 %PIS	50 %PIS
#1	A	18.9	2.04	(0.000, -0.099)	(0.022, -0.073)
	B	18.9	1.98	(0.709, 0.230)	(0.627, 0.374)
	C	18.8	2.07	(-0.562, -0.296)	(-0.532, -0.110)
#2	A	19.0	2.03	(0.023, -0.341)	(0.007, -0.342)
	B	18.8	2.04	(0.685, 0.048)	(0.668, 0.195)
	C	18.7	2.08	(-0.567, -0.401)	(-0.491, -0.261)
#3	A	19.0	2.05	(-0.039, -0.353)	(-0.037, -0.367)
	B	19.0	2.08	(0.611, -0.032)	(0.561, 0.034)
	C	18.9	2.09	(-0.633, -0.420)	(-0.547, -0.254)
#4	A	19.0	2.06	(0.041, -0.321)	(0.088, -0.347)
	B	18.9	2.06	(0.659, 0.020)	(0.707, 0.148)
	C	18.9	2.06	(-0.664, -0.387)	(-0.658, -0.326)
#5	A	19.0	2.04	(0.035, -0.354)	(0.044, -0.403)
	B	19.0	2.06	(0.646, -0.071)	(0.659, -0.050)
	C	18.9	2.07	(-0.603, -0.380)	(-0.503, -0.236)
#6	A	19.0	2.05	(0.150, -0.368)	(0.210, -0.399)
	B	19.0	2.08	(0.730, -0.003)	(0.721, 0.110)
	C	19.0	2.07	(-0.636, -0.398)	(-0.536, -0.255)

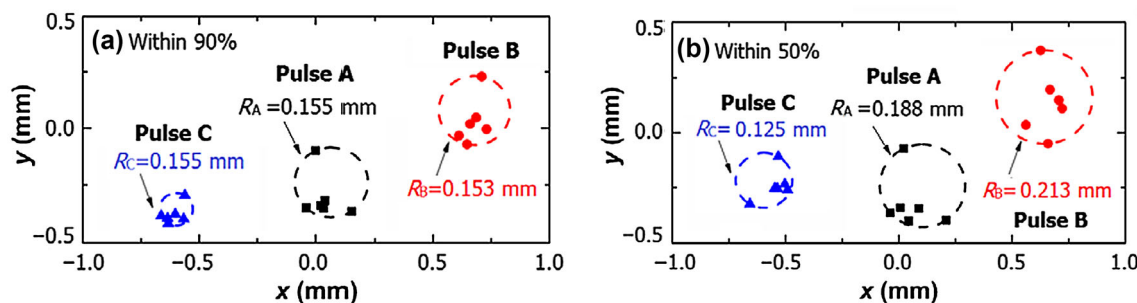


Fig. 4 Spatial jitters of triple-pulse X-ray source centroid, for centroid within 90 % (a) and 50 % (b) PIS boundary

hence a magnification of $M = 4.183$. The experiments are conducted with electron beams of 18.9 MeV and 2.05 kA, trying to maintain a steady and identical state for all pulses.

The pinhole object is placed close to the source to obtain a large magnification so as to acquire image with a better resolution and reduce the image blur effect. According to

the parameters of the pinhole object and the experimental alignment, the view field width for the source reaches 15.7 mm, which is about ten times the source FWHM, so collimating effect of the pinhole object can be neglected.

Typical images of the triple-pulse X-ray source obtained by the pinhole imaging technique are shown in Fig. 3. The conversion ratio of the image pixel to the spatial distance is 0.104 mm/pixel. In order to correct pixel-to-pixel variations of the screen sensitivity and dark current of the camera, a standard procedure for gain and offset modification is applied to the images [21]. Besides, relative displacements of the origin and azimuths of the axes are corrected for different framing images. The source centroids of triple pulses are calculated, considering both the image boundary of 90 %PIS and that of 50 %PIS. The experimental results of X-ray source centroid are listed in Table 2. For each pulse, the center and radius of a minimum circle which contains all centroid positions in different measurements are used to denote the center and the range of source centroid jitters (Fig. 4). For the boundary of 90 %PIS, the jitter radii of the triple-pulse source centroid are 0.155, 0.153 and 0.072 mm for psulses A, B and C, respectively. The deviation distances between the source-jitter centers of each pulse pair are $L_{AB} = 0.690$ mm, $L_{BC} = 1.349$ mm and $L_{AC} = 0.674$ mm. For the boundary of 50 %PIS, the jitter radii are $R_A = 0.188$ mm, $R_B = 0.213$ mm, and $R_C = 0.125$ mm, and the deviation distances are $L_{AB} = 0.673$ mm, $L_{BC} = 1.295$ mm, and $L_{AC} = 0.700$ mm. The spatial jitters of the source centroid are relatively small for each pulse. However, deviations of the source positions are distinct between different pulses, because of, most probably, corkscrew oscillation of the electron beam due to tilted beam injections, inaccurate alignments of solenoid field, and energy spread of the electron beam [22, 23].

5 Conclusion

Spatial jitters of the triple-pulse X-ray source generated by the Dragon-II LIA are measured using the pinhole imaging technique. For flash radiography with a large anti-scatter grid, the spatial jitter of each X-ray pulse and the deviation between different pulses should be smaller than 0.5 mm for reducing direct radiation loss [24]. Numerical simulations are performed for the source position measurement, and the obtained source centroid agrees well with the set one. In each measurement, images of triple pulses are obtained, and the centroids are calculated within 90 %PIS or 50 %PIS boundaries. For each pulse, the spatial jitter of source centroid is small. However, centroids of different pulses deviate distinctively from each other. For a flash radiographic system of large anti-scatter grid to

provide stable and uniform positions of all pulses, the X-ray source should be optimized by reducing the electron beam injection tilt, accurate aligning the magnetic field, and decreasing energy spread of the electron beam.

References

1. T.P. Hughes, D.C. Moir, R.L. Carlson, *Upgrade of the PHER-MEX Accelerator, Conference Record of the 1991 IEEE Particle Accelerator Conference*, vols 1–5 (Accelerator Science and Technology, 1991)
2. P. Allison, M.J. Burns, G.J. Caporaso et al., *Beam-Breakup Calculation for the DARHT Accelerator, Conference Record of the 1991 IEEE Particle Accelerator Conference*, vols 1–5 (Accelerator Science and Technology, 1991)
3. C. Ekdahl, Modern electron accelerators for radiography. *IEEE Trans. Plasma Sci.* **30**, 254–261 (2002)
4. B.T. McCuistian, O. Abeyta, P. Aragon et al., *DARHT-II Commissioning Status, PPC-2003: 14th IFFF International Pulsed Power Conference*, vols 1 and 2 (Digest of Technical Papers, 2003)
5. J. Deng, B. Ding, H. Wang et al., Physical design of the Dragon-I linear induction accelerator. *High Power Laser Part. Beams* **15**, 502–504 (2003). (in Chinese)
6. B.N. Ding, J.J. Deng, H.C. Wang et al., Dragon-I linear induction electron accelerator. *High Energy Phys. Nucl. Phys. Chin. Ed.* **29**, 604–610 (2005). (in Chinese)
7. B. Li, J. Shi, J. Liu et al., Numerical simulation of distribution of scattered exposure and reduced scatter in flash radiographic system. *High Power Laser Part. Beams* **17**, 788–792 (2005). (in Chinese)
8. J. Shi, B. Li, J. Liu et al., Analytic determination of scatter exposure for radiography. *High Power Laser Part. Beams* **18**, 1211–1214 (2006). (in Chinese)
9. J.L. Gerstenmayer, M. Nicolaizeau, P. Vibert, Multihole graded collimator: quantitative tomographic measurements, *Proc. SPIE 1757, Ultrahigh- and High-Speed Photography, Videography, and Photonics*, 40 (1993). doi:10.1117/12.139152
10. F.J. Goldin, S. Mitchell, Collimated step-wedge spectrometer for flash X-ray radiography sources. *Hard X-ray Gamma-ray Detect. Phys. V* **5198**, 126–133 (2004). doi:10.1117/12.503868
11. Z. Xiao, J. Liu, B. Hu et al., Experimental research of the performance of graded collimators in high-energy flash X-ray radiography. *Nucl. Electron. Detect. Technol.* **27**, 512–515 (2007). (in Chinese)
12. S.A. Watson, M. Appleby, J. Klinger et al., *Design, Fabrication and Testing of a Large Anti-Scatter Grid for Megavolt Gamma-ray Imaging, 2005 IEEE Nuclear Science Symposium Conference Record*, Vols 1–5 (2005)
13. T. Tsunoo, N. Nakamori, H. Kanamori et al., The influences of incorrect placement of the focused grid on X-ray image formation. *Phys. Med. Imaging* **3336**, 651–659 (1998). doi:10.1117/12.317070
14. Y. Kiwamoto, Y. Kikuchi, T. Takahashi et al., Pinhole camera imaging of X-rays and energetic neutral atoms for hot plasma diagnostics. *Rev. Sci. Instrum.* **69**, 2574–2575 (1998). doi:10.1063/1.1148962
15. W. Leitenberger, H. Wendrock, L. Bischoff et al., Pinhole interferometry with coherent hard X-rays. *J. Synchrotron Radiat.* **11**, 190–197 (2004). doi:10.1107/s0909049503029169
16. E. Samei, M.J. Flynn, D.A. Reimann, A method for measuring the presampled MTF of digital radiographic systems using an

- edge test device. *Med. Phys.* **25**, 102–113 (1998). doi:[10.1118/1.598165](https://doi.org/10.1118/1.598165)
17. C. Ekdahl, Characterizing flash-radiography source spots. *J. Opt. Soc. Am. A Opt. Image Sci. Vis.* **28**, 2501–2509 (2011)
 18. S. Agostinelli, J. Allison, K. Amako et al., GEANT4—a simulation toolkit. *Nucl. Instrum. Methods Phys. Res., Sect. A* **506**, 250–303 (2003). doi:[10.1016/s0168-9002\(03\)01368-8](https://doi.org/10.1016/s0168-9002(03)01368-8)
 19. D. Sardari, R. Maleki, H. Samavat et al., Measurement of depth-dose of linear accelerator and simulation by use of Geant4 computer code. *Rep. Pract. Oncol. Radiother.* **15**, 64–68 (2010). doi:[10.1016/j.rpor.2010.03.001](https://doi.org/10.1016/j.rpor.2010.03.001)
 20. J.M. Boone, J.A. Seibert, An analytical edge spread function model for computer fitting and subsequent calculation of the LSF and MTF. *Med. Phys.* **21**, 1541–1545 (1994). doi:[10.1118/1.597264](https://doi.org/10.1118/1.597264)
 21. A. Karellas, L.J. Harris, H. Liu et al., Charge-coupled device detector—performance considerations and potential for small-field mammographic imaging applications. *Med. Phys.* **19**, 1015–1023 (1992). doi:[10.1118/1.596819](https://doi.org/10.1118/1.596819)
 22. Y.J. Chen, Corkscrew modes in linear accelerators. *Nucl. Instrum. Methods Phys. Res., Sect. A* **292**, 455–464 (1990). doi:[10.1016/0168-9002\(90\)90403-s](https://doi.org/10.1016/0168-9002(90)90403-s)
 23. W. Zhang, Z. Dai, H. Li et al., *Beam Instability and Correction for “Dragon-I”, 2007 IEEE Particle Accelerator Conference*, vols 1–11 (2007)
 24. H.B. Xu, Y. Ye, N. Zheng, Influence of source out of focused grid on image in high-energy X-ray radiography. *High Power Laser Part. Beams* **27**, 115103 (2015). doi:[10.11884/HPLPB201527.115103](https://doi.org/10.11884/HPLPB201527.115103). **(in Chinese)**